Inorganica Chimica Acta 582 (2025) 122684

Contents lists available at ScienceDirect

Inorganica Chimica Acta

journal homepage: www.elsevier.com/locate/ica

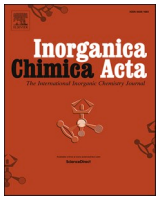

Synthesis and crystallographic investigation of two new neutral Ir(III) complexes bearing 6-(phenyl)phenanthridine ligands☆

Luigi Menduti [a,1], Matteo Mori [a,1], Xuequan Zhou [b], Nicolò Quadrio [a,c], Fiorella Meneghetti [a,*], Luisa De Cola [a,b]

[a] Department of Pharmaceutical Sciences, University of Milan, via L. Mangiagalli 25, 20133 Milano, Italy
[b] Department of Biochemistry, Istituto di Ricerche Farmacologiche Mario Negri IRCCS, Via M. Negri 2, 20156 Milano, Italy.
[c] Department of Chemistry, Biology and Biotechnology, University of Perugia, Via dell'Elce di Sotto 8, 06123 Perugia, Italy.

ARTICLE INFO

Keywords:
Iridium(III) complexes
Cyclometalating ligands
Pyridyl-triazole/pyridyl-pyrazole
Single-crystal X-ray diffraction
Photophysical properties

ABSTRACT

Herein, we report two new iridium(III) complexes (**1** and **2**), featuring 6-(phenyl)phenanthridine derivatives as cyclometalating (CˆN) ligands and pyridyl-triazole or pyridyl-pyrazole ancillary (LˆX) ligands. The synthesis of the two compounds was performed by reaction of the 6-(phenyl)-phenanthridine chloro-bridged dimer with the pyridyl-triazole/pyridyl-pyrazole (LˆX) ligand. Single crystals of both complexes (**1** and **2**) were grown and analyzed by X-ray diffraction. Full crystallographic characterization and comparison of **1** and **2** solid-state structures is reported. Spectroscopic characterization revealed similar emissive properties for **1** (λ_{max} = 650 nm; τ_{deg} = 1.43 μs, QY_{deg} = 11.6 %) and **2** (λ_{max} = 660 nm; τ_{deg} = 1.45 μs, QY_{deg} = 12.1 %).

1. Introduction

Cyclometalated Ir(III) complexes, extensively studied as emitters in organic light-emitting diodes (OLEDs) [1–3], have recently gained significant attention for applications in electrochemiluminescence (ECL) and ECL-based immunoassays [4–6]. Compared to Ru complexes, these systems offer higher emission quantum yields and greater flexibility in tuning emission energies through modifications of the cyclometalated (CˆN) ligands [7–10]. Within the broader class of iridium cyclometalated complexes, those incorporating phenylphenanthridine CˆN ligands are particularly efficient in terms of photophysical performances, showing bright red emission due to their π-extended scaffold [7,11–13]. Our group has a long-standing expertise in phenanthridine-based iridium complexes and, in recent years, has contributed to this field through reports on the synthesis and application of these compounds in ECL and cell imaging [14–17]. However, few reports provide detailed crystallographic studies of Ir(III) complexes bearing such rigid and highly conjugated CˆN ligands [7,14].

Herein, we report the synthesis and full crystallographic characterization of two novel 6-(phenyl)phenanthridine-based iridium complexes, **1** and **2** (Fig. 1).

The two complexes feature two different five-membered ancillary ligands, namely a pyridyl-1,2,4-triazole (**1**) and a pyridyl-pyrazole (**2**). These LˆX ligands were selected to assess the effect of the replacement of one N atom with a C atom in the azole moiety (triazole → pyrazole) on the structural characteristics of the corresponding complexes. Additionally, different functionalization on the pyridyl-triazole (hydroxyl group: **1**) and pyridyl-pyrazole (carboxylic acid methyl ester: **2**) ligands was chosen to evaluate the influence of hydrogen bonding and electron-donating/electron-withdrawing groups on the molecular geometry. Spectroscopic studies were also performed to corroborate the lack of effect of LˆX ancillary ligands on the absorption/emission properties of the complexes.

2. Results and discussion

2.1. Synthesis of complexes 1 and 2

The synthesis of the iridium complexes **1** and **2** is shown in Scheme 1. The cyclometalating ligand 6-(phenyl)phenanthridine **3** was prepared on a gram scale *via* a Pictet-Spengler reaction, starting from the commercially available biphenylamine and benzaldehyde in

☆ This article is part of a Special issue entitled: 'Alberto Albinati' published in International Journal of Cardiology.

* Corresponding author.
E-mail address: fiorella.meneghetti@unimi.it (F. Meneghetti).

[1] These authors contributed equally to this work.

https://doi.org/10.1016/j.ica.2025.122684
Received 29 January 2025; Received in revised form 18 March 2025; Accepted 27 March 2025
Available online 28 March 2025

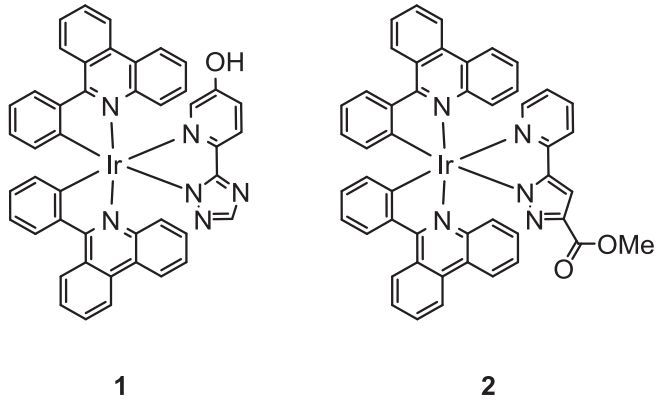

Fig. 1. Structure of the Ir(III) complexes (**1** and **2**) investigated in this work.

trifluoroacetic acid (TFA) at 140 °C (see Supporting Information, SI) [18]. Compound **3** was therefore reacted with $IrCl_3(H_2O)_3$ in the Nonoyama reaction [19] to give the corresponding chloro-bridged Ir(III) dimer **4** in 45 % yield (Scheme 1), using a protocol previously reported by our group [14].

Then, the chloro-bridged dimer **4** was treated with intermediate **5** (for its preparation, see SI) in DCM/MeOH (2:1) at 50 °C, in the presence of Na_2CO_3. The pure complex **1** was obtained in 48 % yield after chromatographic purification. Using a similar procedure, **4** was reacted with the commercially available methyl 5-(pyridin-2-yl)-1*H*-pyrazole-3-carboxylate, giving **2** in 74 % yield (Scheme 1).

2.2. Crystallographic characterization of 1 and 2

The solid-state structures of complexes **1** and **2** were studied by single-crystal X-ray diffraction. Crystals of **1** were successfully grown as small orange blocks through slow evaporation of a chloroform solution containing the complex. For **2**, well-formed ruby-red blocks were obtained by layering hexane onto a solution of the complex in acetonitrile/methanol.

Both complexes crystallized in the monoclinic system, with centrosymmetric space group $P2_1/c$; their molecular structures are presented in Fig. 2, as thermal ellipsoid models. Notably, the asymmetric unit of **2**

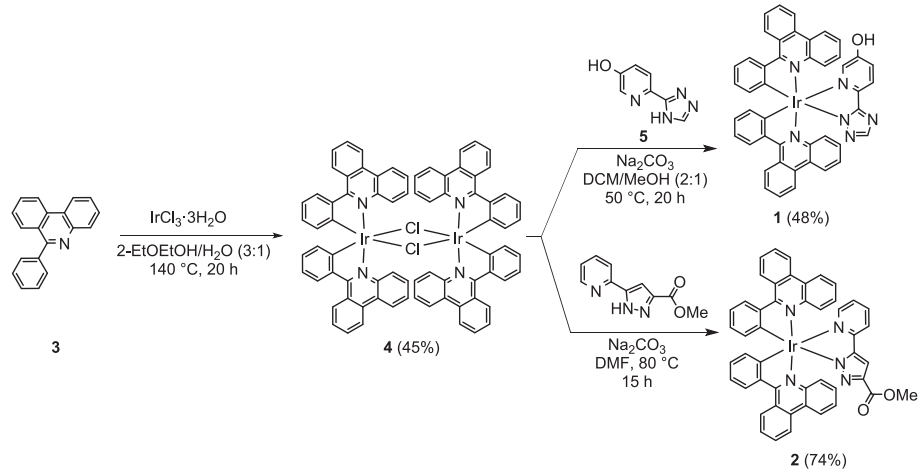

Scheme 1. Synthesis of the Iridium complexes **1** and **2**. Ligand **5** is not known in the literature and was synthesized in one step following a procedure reported for similar pyridyl-triazole systems (see SI) [20].

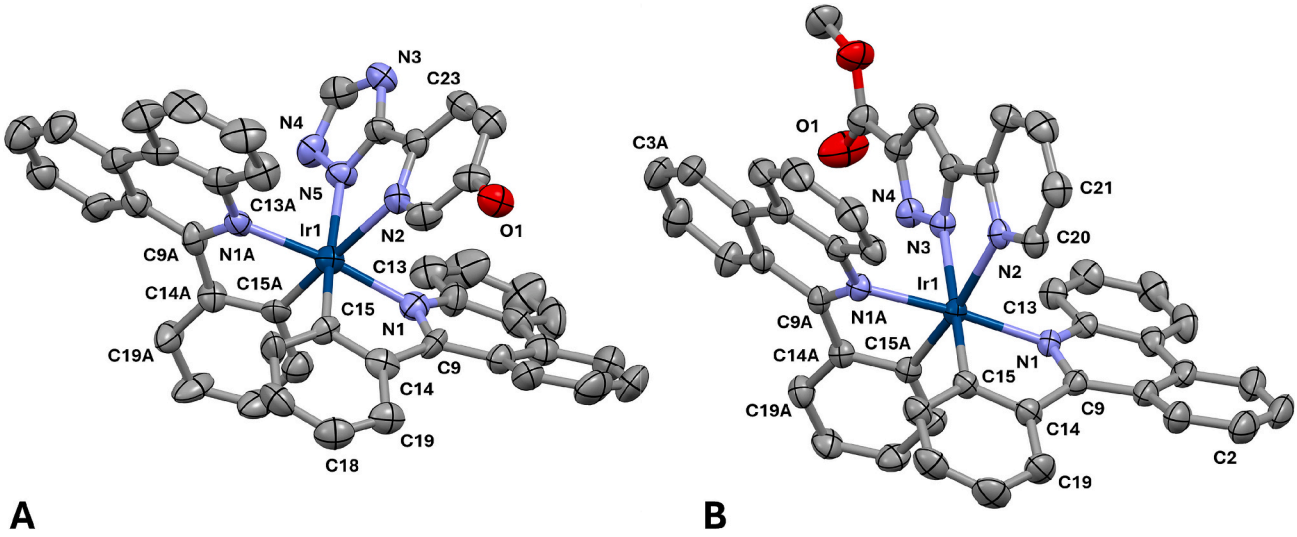

Fig. 2. Thermal ellipsoid diagram of **1** (**A**) and **2** (**B**), with the arbitrary atom-numbering scheme. Displacement ellipsoids are drawn at the 40 % probability level. In the discussion, the two 6-(phenyl)phenanthridine ligands of both complexes are designated as either "X" (atoms indicated only by numbers) or "Y" (atoms indicated by numbers followed by "A"). Hydrogen atoms and the acetonitrile molecule in **2** are omitted for the sake of clarity.

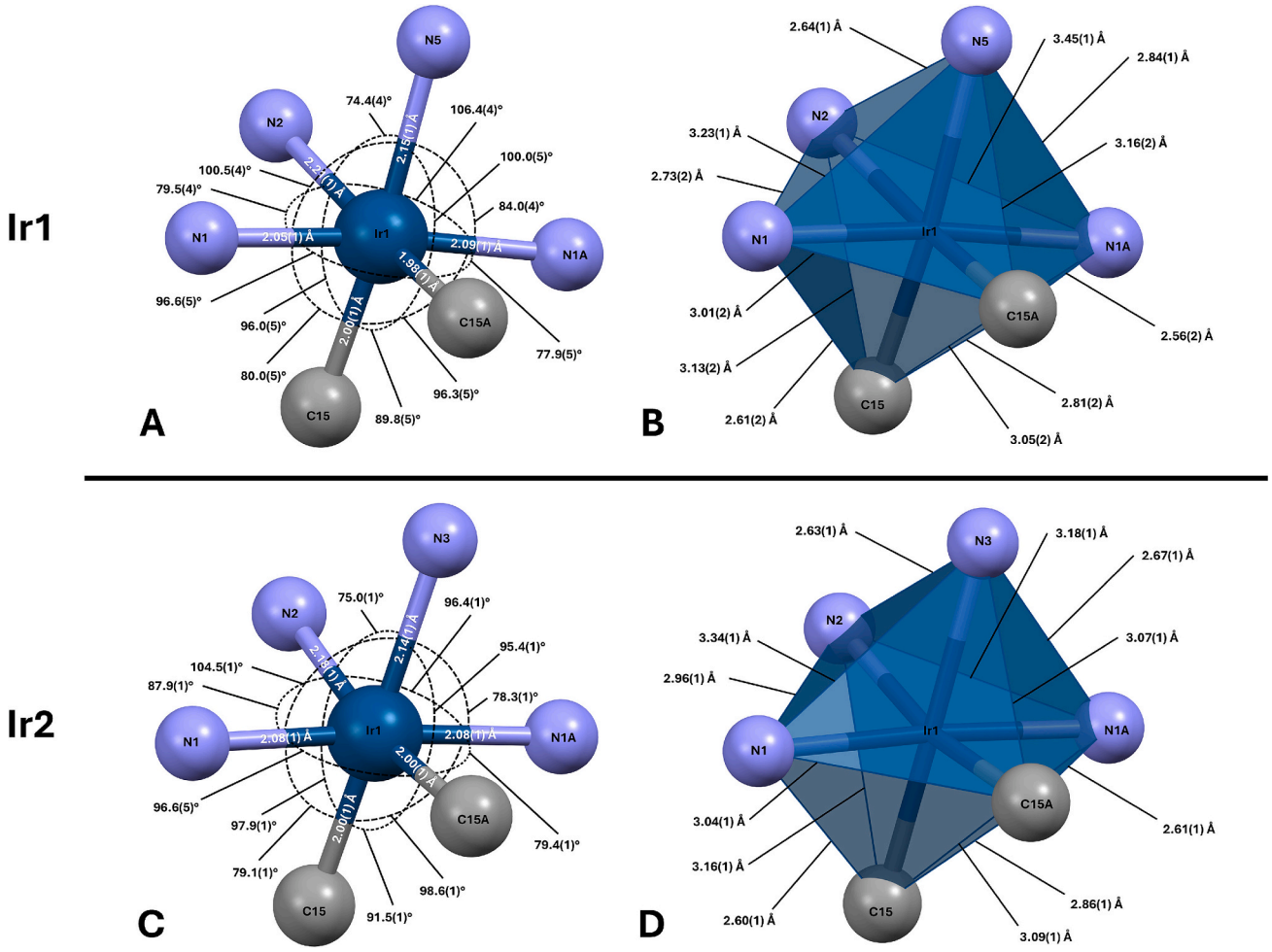

Fig. 3. Distances (Å) and angles (°) within the Ir(III)-coordination sphere and edge lengths of the coordination polyhedron for **1** (**A**,**B**) and **2** (**C**,**D**).

also features an acetonitrile molecule.

In **1**, the Ir(III) center is hexacoordinated by atoms N1, N1A, N2, N5, C15, and C15A, with the chelating ligands consisting of two 6-phenylphenanthridine molecules and one 6-(3*H*-1,2,4-triazol-3-yl)pyridin-3-ol molecule. The metal displays a distorted octahedral geometry, due to a series of factors, including the *trans* configuration of the complex, the limited bite angles of the chelating ligands, and the overall steric bulkiness of the molecules. The distances between the metal and N1, N1A, and C15 are 2.05 (1) Å, 2.09 (1) Å, 2.00 (1) Å, respectively. These values fall within the average limits for similar Iridium complexes, as shown by the CSD Mogul routine [21–23]. The Ir1-C15A bond is slightly shorter than the average, with 1.98 (1) Å. Conversely, the distances between the metal center and N2 and N5 are significantly elongated, with values of 2.21 (1) Å and 2.15 (1) Å, respectively. Both these atoms belong to the smaller pyridine-3-ol ligand, which is pushed farther from the metal center by the steric hindrance of the 6-phenylphenanthridine chelators. The angles also vary significantly from the ideal value, with the maximum deviations observed for N2-Ir1-N5 and N2-Ir1-N1A, measuring 74.4 (4)° and 106.4 (4)°, respectively. Overall, seven angles are below the 90° threshold, while five are above it. As expected, when a single ligand coordinates to the metal center through two spatially close donor atoms, it imposes a small bite angle, resulting in coordination angles smaller than 90°. In contrast, when the coordinating atoms originate from different ligands, this geometric constraint is absent, allowing the steric and electronic demands of the complex to drive an expansion of the angles (>90°) as a compensatory adjustment. This distortion helps preserve the overall stability of the coordination environment. As a result of these variations, the geometry of the octahedron undergoes considerable distortion from its ideal configuration (Fig. 3A, B). This can be further observed by analyzing the inclination of the three planes passing through the center and the opposite vertices of the polyhedron. Given the best mean planes *A* (N2-N1-Ir1-C15A-N1A), *B* (N2-C15-Ir1-C15A-N5), and *C* (N1-C15-Ir1-N1A-N5), the angles *A*-*B*, *A*-*C*, and *B*—*C* are 79.9°, 79.2°, and 76.9°, respectively. The maximum deviation from plane *A* is observed at C15A (0.10 Å), for plane *B* at N2 (0.08 Å), and for plane *C* at C15 (0.16 Å). Conversely, the metal center lies almost exactly on the three planes, with minimal deviations of 0.03 Å, 0.02 Å, and 0.04 Å for planes *A*, *B*, and *C*, respectively.

The geometry of complex **2** is very similar to that of **1** (Fig. 3C,D), with the Ir(III) center hexacoordinated by atoms N1, N1A, N2, N3, C15, and C15A, belonging to two 6-phenylphenanthridine molecules and one methyl 5-(pyridin-2-yl)-1*H*-pyrazole-3-carboxylate molecule. The distances between the metal and the coordinating atoms are as follows: Ir1-N1: 2.08 (1) Å, Ir1-N1A: 2.08 (1) Å, Ir1-N2: 2.18 (1) Å, Ir1-N3: 2.14 (1) Å, Ir1-C15: 2.00 (1) Å, Ir1-C15A: 2.00 (1) Å. These values are consistent with the previous structure and fall within the average range based on CSD Mogul analysis [21]. The distortion of the octahedron is evident from the coordination angles, with the maximum deviations from the ideal value observed for N2-Ir1-N3 and N1-Ir1-N3, measuring 75.0 (1)° and 104.5 (1)°, respectively. Overall, five angles are below the 90° threshold, while seven are above it. This represents a variation from **1**, indicating a slightly different orientation of the ligands. This can be further observed by the inclination of the coordination planes. Considering *A* (N2-N1-Ir1-C15A-N1A), *B* (N2-C15-Ir1-C15A-N3), and *C* (N1-C15-Ir1-N1A-N3), the angles *A*-*B*, *A*-*C*, and *B*—*C* are 77.4°, 81.1°, and 82.1°, respectively. The maximum deviation from plane *A* is observed at

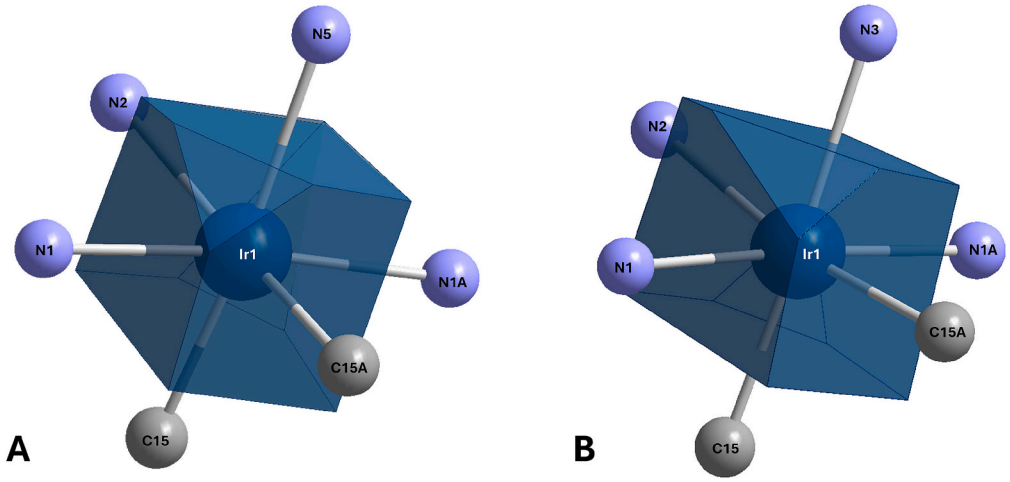

Fig. 4. VDP built around Ir(III) for **1** (**A**) and **2** (**B**). For clarity, only coordinating atoms are shown.

Table 1
Details of the VDP generated around Ir(III) for **1** and **2**, as calculated by *Diamond*.

Atom (Ir1)	Distance (Å)	SA (%)	Atom (Ir2)	Distance (Å)	SA (%)
C15A	1.98(1)	17.33	C15	2.00(1)	17.38
C15	2.00(1)	17.10	C15A	2.00(1)	17.08
N1	2.05(1)	15.80	N1	2.08(1)	16.04
N1A	2.09(1)	15.39	N1A	2.08(1)	15.34
N5	2.15(1)	15.07	N3	2.14(1)	14.25
N2	2.21(1)	13.57	N2	2.18(1)	14.77
H13A	2.92(1)	3.25	H13	2.86(1)	3.04
H13	2.93(1)	2.48	H13A	2.99(1)	2.06
CN	6		CN	6	
Rsd (Å)	1.29		Rsd (Å)	1.29	
V ($Å^3$)	9.05		V ($Å^3$)	9.02	

C15A (0.12 Å), for plane *B* at N3/C15 (0.03 Å), and for plane *C* at C15 (0.12 Å). These values are very close to those of **1**. Similarly, the minimal deviations of the metal center relative to the three planes – 0.05 Å, 0.05 Å, and 0.03 Å for planes *A*, *B*, and *C*, respectively – remain also quite consistent.

The coordination topology of **1** was further examined by means of the Voronoi-Dirichlet tessellation of the space around the Ir(III) atom (Fig. 4) [24,25]. The Voronoi-Dirichlet polyhedron (VDP) of an atom A, surrounded by atoms X, is a convex polyhedron centered on atom A [26]. The VDP is bounded by planes that perpendicularly bisect the lines connecting A to each surrounding atom X at their midpoints. This method can be conveniently used to calculate the coordination number (CN) in metal crystals [27]. According to the Frank-Kasper definition of an atomic domain, the CN corresponds to the number of faces of the VDP. More specifically, each atom neighboring the metal influences the CN based on the solid angle (SA) of the corresponding face, with only the largest SAs significantly contributing to a full unit of the CN (SA > 10 %) [27]. In this case, the iridium atom is coordinated by N1, N1A, N2, N5, C15, and C15A (CN = 6), as confirmed by interatomic distances and SAs, which are detailed in Table 1. Other neighboring atoms exhibit smaller SAs and greater distances, which are insufficient to meaningfully affect the CN. The same conclusions can be drawn from the analysis of complex **2**, in which the iridium atom exhibits a CN = 6, involving N1, N1A, N2, N3, C15, and C15A (Table 1, Fig. 4).

Regarding the ligands of **1**, the phenanthridine portion of the 6-phenylphenanthridine molecules is nearly planar, although it exhibits significant strain and deformation for an aromatic system. The maximum deviations from the best mean planes are observed at C9 (0.24 Å) and N1A (0.39 Å) in moieties X and Y, respectively. In X, the 6-phenyl substituent is inclined at 32.0° relative to the plane of the phenanthridine (torsional angle N1-C9-C14-C19: 160 (1)°), while in Y it is inclined at 26.0° (torsional angle N1A-C9A-C14A-C19A: 158 (1)°). Conversely, the smaller 6-(3*H*-1,2,4-triazol-3-yl)pyridin-3-ol ligand is almost perfectly planar, with the maximum deviation from the mean plane observed at the iridium-coordinating atom N5 (0.11 Å). Overall, the interaction of the six neighboring atoms with the metal induces minor strains in the structure of the three ligands, resulting in some bond lengths and angles deviating from typical values. Overall, the conformational tension in **2** appears to be less pronounced, with no significant variations from average structural parameters. Although the phenanthridine cores are not completely flat, they deviate less from planarity, with the maximum displacements observed at C9 (0.17 Å) and N1A (0.17 Å). In X, the 6-phenyl substituent is inclined at 25.7° relative to the plane of the phenanthridine (torsional angle N1-C9-C14-C19: 161.0 (2)°), while in Y it is inclined at 32.1° (torsional angle N1A-C9A-C14A-C19A: 156.5 (2)°). Similarly to **1**, the ancillary ligand is almost flat, with the maximum deviation observed at N2 (0.10 Å). A superimposition of the two complexes is shown in Fig. 5.

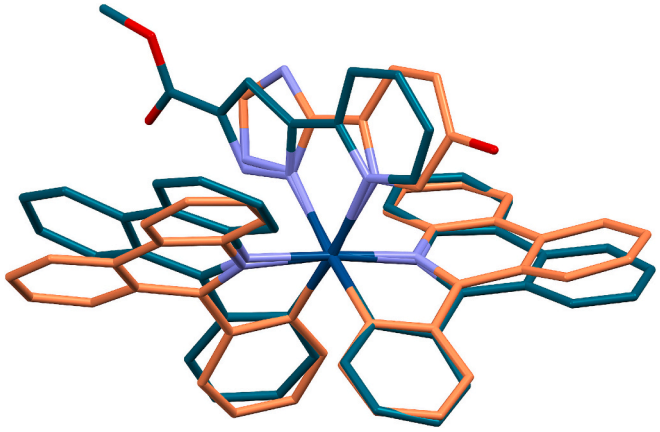

Fig. 5. Superimposition of the stick models of **1** (C atoms in amber) and **2** (C atoms in teal). Hydrogen atoms are omitted for clarity. (For interpretation of the references to colour in this figure legend, the reader is referred to the web version of this article.)

The main force driving the intermolecular packing in **1** is an H-bond established between the hydroxyl group (O1-H1) of the pyridin-3-ol ligand and N3, belonging to the triazole moiety of an adjacent complex (Fig. 6A). This interaction leads to the formation of chains extending along the *b* axis. Weaker CπH···X (with X = N, O) bonds contribute not only to the intermolecular network, but also to the stabilization of the metal complex [28]. Due to the presence of an ester

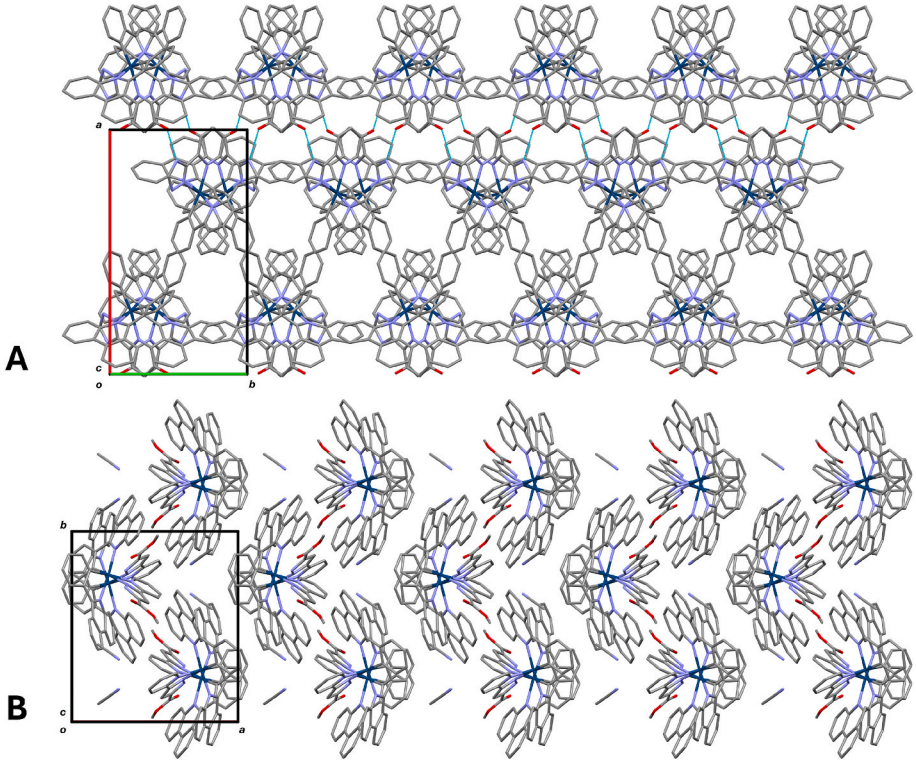

Fig. 6. Stick model showing the crystal packing of **1** (**A**) and **2** (**B**), viewed along the *c* axis. The main H-bond in **1** is represented with a cyan line. The π-π stacking interactions can be inferred from the overlap of the aromatic systems. For the sake of clarity, hydrogen atoms are omitted. (For interpretation of the references to colour in this figure legend, the reader is referred to the web version of this article.)

Table 2
H-bond geometry (D: Donor, A: Acceptor) for **1** and **2**. Atom labels are shown in Fig. 2 (N5 in **2** refers to the acetonitrile nitrogen).

	D-H/Å	H•••A/Å	D•••A/Å	D-H•••A/°	Equivalent positions
1					
C13A-H13A···N2^{I}	0.93(2)	2.38(1)	3.17(2)	143(1)	
C13-H13···N4^{I}	0.93(1)	2.72(1)	3.53(2)	146(1)	
O1-H1B···N3^{II}	0.82(1)	1.82(1)	2.62(2)	166(1)	^{I}x, y, z; ^{II}-x, y + 1/2, 1/2-z; ^{III}-x, y-1/2, 1/2-z; ^{IV}x, 1/2-y, z-1/2
C23-H23···O1^{III}	0.93(2)	2.82(1)	3.65(2)	149(1)	
C18-H18···N4^{IV}	0.93(2)	2.89(3)	3.65(2)	139(1)	
2					
C13-H13···N3^{I}	0.93(2)	2.32(1)	3.06(1)	134(1)	
C13-H13···N4^{I}	0.93(2)	2.51(1)	3.39(1)	157(1)	
C20-H20···O1^{II}	0.93(2)	2.85(1)	3.45(1)	123(1)	^{I}x, y, z; ^{II}x, 3/2-y, z-1/2; ^{III}-x, 1-y, 2-z; ^{IV}-x, y + 1/2, 3/2-z
C21-H21···O1^{II}	0.93(2)	2.74(1)	3.39(1)	127(1)	
C3A-H3A···N5^{III}	0.93(2)	2.95(1)	3.82(1)	155(1)	
C2-H2···N5^{IV}	0.93(2)	2.84(1)	3.49(1)	128(1)	

group in **2**, the crystal packing does not rely on the formation of any strong H-bond. Only weak CπH···X (with X = N, O) interactions are observed, most of which show suboptimal lengths and angles. The co-crystallized solvent does not play any significant role in the stabilization of the structure either. A complete account of H-bonds is provided in Table 2.

Due to the large number and considerable size of the aromatic systems in **1**, π-π stacking plays a significant role in the packing, with parallel displaced (centroid-centroid distances: 3.98 Å), T-shaped (centroid-centroid distances: 4.95 Å), and inclined edge-to-face (centroid-centroid distances: 4.01, 4.08, 4.93 Å) interactions (Fig. 6A) [29]. In **2**, π-π stacking is also a major contributor in packing stabilization (Fig. 6B), with a strong parallel displaced interaction between the phenanthridine cores of neighboring complexes along the *a* axis (minimal centroid-centroid distance: 3.72 Å). The presence of the H-bond in **1** may contribute to bringing the molecules closer together, potentially leading to the more intricate π-π stacking network observed. In contrast, the absence of a similar short-range bond in **2**, combined with the presence of the co-crystallized acetonitrile molecule, may explain the occurrence of a single π-π stacking interaction, which, nonetheless, remains rather strong and serves as the main determinant of the packing.

The intermolecular interactions in **1** were further analyzed by computing the Hirshfeld Surface (HS) of the complex (V = 878.62 Å^3; A = 633.53 Å^2; $G = 0.700$; $\Omega = 0.074$) [30]. The HS was mapped over the normalized contact distance (d_{norm}), according to the following equation:

$$d_{norm} = \frac{d_i - r_i^{vdW}}{r_i^{vdW}} + \frac{d_e - r_e^{vdW}}{r_e^{vdW}}$$

where d_i is the distance between the HS and the nearest nucleus inside the surface, d_e is the distance between the HS and the nearest nucleus outside the surface, and r^{vdW} represents the van der Waals radius of the atom [30,31]. The d_{norm} property (Fig. 7A), visualized with the

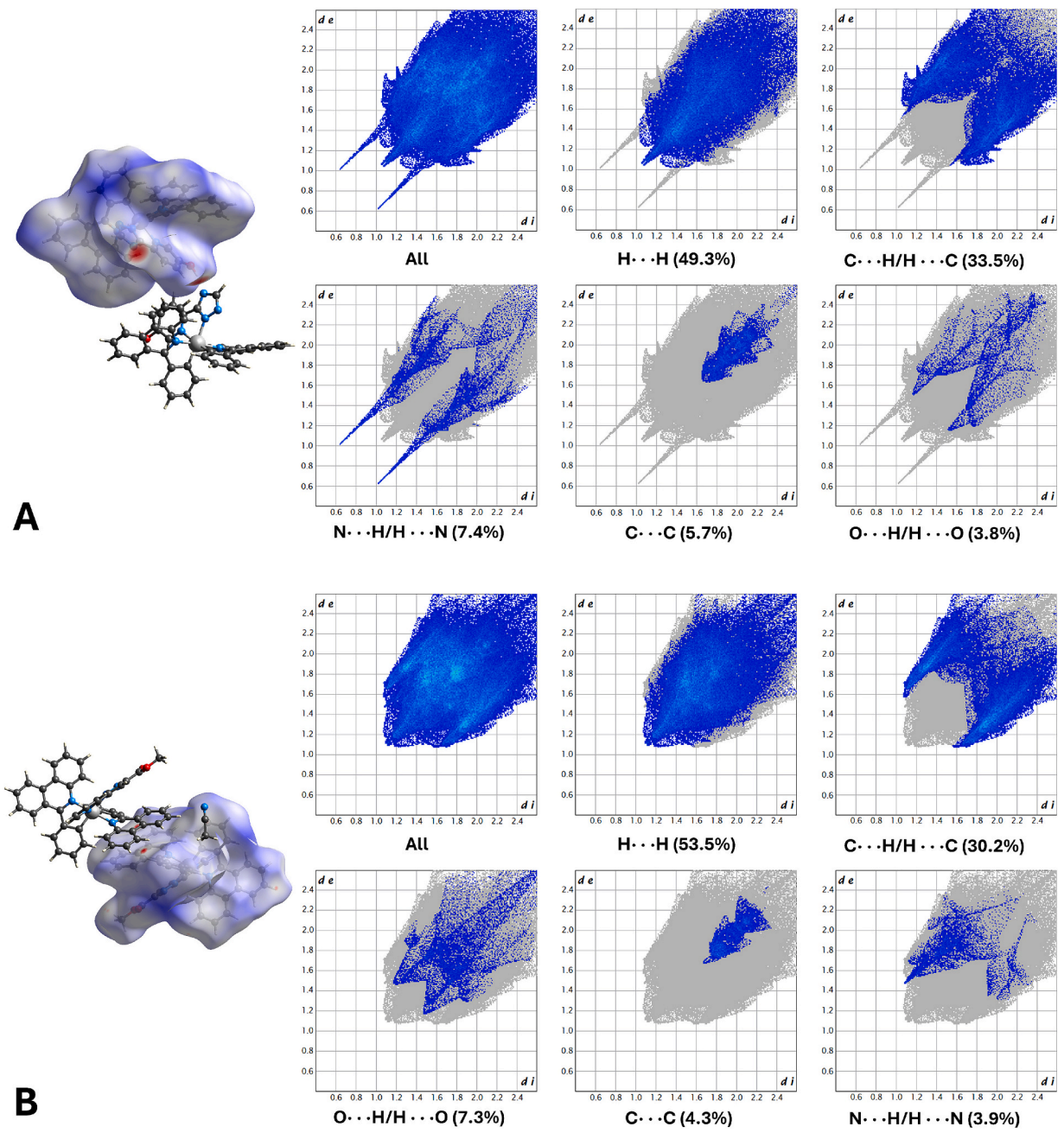

Fig. 7. HS of **1** (**A**) mapped over the d_{norm} property (left) with a fixed colour scale in the range − 0.7546 au (red) – 2.1849 au (blue). Red, blue, and white indicate intermolecular contacts shorter, longer, and approximately equal to the sum of their van der Waals radii, respectively. 2D Fingerprint plots of **1** (right), providing a visual summary of the frequency of each combination of d_e and d_i across the HS. Points with a contribution to the surface are colored blue for a small contribution to green for a great contribution; HS of **2** (**B**) mapped over the d_{norm} property (left) with a fixed colour scale in the range − 0.0851 au (red) – 2.5921au (blue). 2D Fingerprint plots of **2** (right). (For interpretation of the references to colour in this figure legend, the reader is referred to the web version of this article.)

traditional red-white-blue colour scheme, shows a prevalence of white-blue areas, indicating intermolecular contacts that are longer than or equal to the sum of the van der Waals radii of neighboring atoms. Two intense red spots represent the short-range H-bond between the hydroxyl group and the triazole nitrogen, while fainter regions indicate the presence of minor, non-traditional H-bonds. The presence of the O1-H1B···N3 contact is further visualized by two long spikes protruding towards the lower left part of the 2D fingerprint plot of the HS (Fig. 7A). The graph indicates that the most prevalent contacts are H···H (49.3 %), followed by C···H/H···C (33.5 %), which occupy the "wings" of the plot and can be partially attributed to non-traditional π-π stacking. Interestingly, the region corresponding to H···H contacts extends at low d_e/d_i values, suggesting the presence of short-range van der Waals interactions. The HS was also computed for **2** (V = 939.26 Å^3; A = 654.58 Å^2; $G = 0.709$; $\Omega = 0.061$). The d_{norm} property confirms the absence of strong interactions, with a surface largely characterized by white/blue areas (Fig. 7B). The few small red spots are mainly the result of weak or random close contacts. This is further supported by the analysis of the 2D plot, which displays a compact shape without significant spikes or protrusions (Fig. 7B). Most of the surface is occupied by H···H contacts (53.5 %), followed by C···H/H···C (30.2 %), O···H/H···O (7.3 %), C···C (4.3 %), and N···H/H···N (3.9 %).

When analyzing HSs, the calculation of the enrichment ratios can provide valuable insights into how certain atom-atom interactions

Table 3
Analysis of the intermolecular contacts on the HSs of **1** and **2**. Contact values were computed with *CrystalExplorer*. Surface contributions and enrichment ratios were calculated according to Jelsch [32].

	1					**2**				
Atoms	**H**	**C**	**N**	**O**	**Ir**	**H**	**C**	**N**	**O**	**Ir**
Surface (%)	71.7	22.6	3.9	2.0	0	74.2	19.8	2.0	4.0	0
Contacts (%)										
H	49.3					53.5				
C	33.5	5.7				30.2	4.3			
N	7.4	0.3	0			3.9	0.1	0		
O	3.8	0	0	0.1		7.3	0.7	0	0	
Ir	0	0	0	0	0	0	0	0	0	0
Enrichments										
H	0.95					0.97				
C	**1.03**	**1.10**				**1.03**	**1.10**			
N	**1.32**	0.17	–			**1.31**	–	–		
O	**1.32**	–	–	–		**1.23**	0.44	–	–	
Ir	–	–	–	–	–	–	–	–	–	–

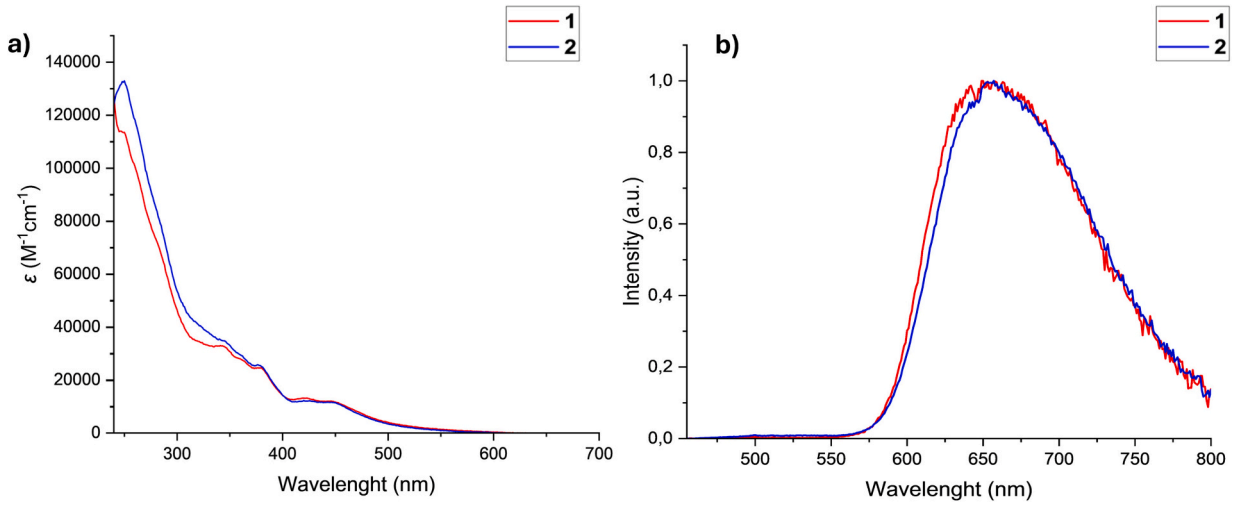

Fig. 8. a) Molar absorptivity of **1** (red traces) and **2** (blue traces) in MeOH; **b)** emission spectra of **1** (red traces) and **2** (blue traces) in MeOH at room temperature. λ_{exc} = 435 nm. Samples concentration: 8 × 10^{-5} M. (For interpretation of the references to colour in this figure legend, the reader is referred to the web version of this article.)

Table 4
Photophysical properties of **1** and **2** in MeOH.

			Air				***Degassed***		
	λ_{abs} **[nm]**	λ_{em} **[nm]**	$QY^{[a]}$ **[%]**	$\tau^{[a]}$ **[μs]**	$k_r/k_{nr}^{[b]}$ **(x10^5) [s^{-1}]**		$QY^{[c]}$ **[%]**	$\tau^{[c]}$ **[μs]**	$k_r/k_{nr}^{[b]}$ **(x10^5) [s^{-1}]**
1	249, 345, 380, 428, 450	650	1.9	0.25	0.62/41.9		11.6	1.43	0.8/6.1
2	249, 345, 380, 428, 450	660	1.4	0.235	0.81/41.7		12.1	1.45	0.84/6.1

[a] Emission quantum yields (QY) and excited state lifetimes (τ) measured in MeOH air-equilibrated solutions. [b] radiative (k_r) non-radiative (k_{nr}) constants calculated as follows: $k_r = QY/\tau$; $k_r = (1\text{-}QY)/\tau$. [c] Emission quantum yield (QY) and lifetime (τ) measured in degassed MeOH solutions. Plots of the emission decays of **1** and **2** are given in the Supporting Information.

deviate from random occurrence, thus revealing the preferences and driving forces behind molecular packing in crystals [32]. The analysis of these parameters revealed that N···H/H···N, O···H/H···O, C···H/H···C, and C···C contacts are favored in both **1** and **2**, essentially confirming the previous analysis of the intermolecular networks of the crystals (Table 3).

2.3. Photophysical properties

Alongside the crystallographic characterization, we performed spectroscopic studies to evaluate the absorption/emission properties of the two new complexes **1** and **2**.

The UV − vis absorption spectra of **1** and **2** (Fig. 8a, Table 4) were recorded at room temperature in MeOH solutions. Due to their similar structure (same cyclometalating (CˆN) ligand), **1** and **2** showed very similar absorption profiles. In detail, in the high energy region (250–400 nm), both **1** and **2** showed maxima at 249 nm attributed to the high-energy azole moiety and lower intensity bands at 345 and 380 nm, which can be assigned to π − π* transitions localized on the CˆN ligands. Lower energy bands (peaked at 428, 450 nm) are responsible for spin-allowed singlet and triplet metal-to-ligand charge transfer (MLCT) transitions involving the iridium center and the pyridine ring of the CˆN

phenanthridine ligand, according to what reported for similar complexes [10,14,15,33]. The lowest band is assigned to spin-forbidden singlet-to-triplet absorption, partially allowed because of the strong spin-orbit coupling given by the heavy iridium atom.

Both **1** and **2** displayed bright red emission in MeOH (Fig. 8b, Table 4); **1**, bearing a pyridyl-triazole ancillary ligand (LˆX), showed an emission maximum at 650 nm, while **2**, bearing a pyridyl-pyrazole ligand, has a slightly red-shifted broad emission band (λ_{max} = 660 nm; Fig. 8b and Table 4). The two complexes show very similar emission lifetimes (τ_{air} = 250 ns / τ_{deg} = 1.43 μs for **1** and τ_{air} = 235 ns/τ_{deg} = 1.45 μs for **2**) and emission quantum yields (QY_{air} = 1.9 % / QY_{deg} = 11.6 % for **1** and QY_{air} = 1.4 % / QY_{deg} = 12.1 % for **2**). In aerated media, both lifetimes and QYs become shorter (Table 4), as expected for triplet emitters (quenched by dioxygen). **1** and **2** emissions are generated by a mixing of ^{3}LC and ^{3}MLCT involving the 6-(phenyl)phenanthridine chelate. However, as already reported for similar complexes [14,15], the rather short-excited state lifetimes in both aerated and degassed solutions suggest a more ^{3}MLCT character. Taken together, the spectroscopic characterizations indicate that the large π-system of the 6-(phenyl) phenanthridine CˆN ligand (**1**) provides redshifted emission with respect to complexes bearing less π-extended ligands (*e.g.*, phenyl quinoline (pq), phenylpyridine (ppy)) and, in turn, **2**). The two ancillary ligands act as spectator chromophores (singlet/triplet energies higher than those of CˆN ligands) according to what observed for similar phenanthridine complexes reported by our group [14,15].

Overall, our studies on **1** and **2** show that the introduction of pyridyl-triazole or pyridyl-pyrazole LˆX ancillary ligands have negligible effect on the emissive excited state of 6-(phenyl)-phenanthridine complexes, thus providing a tool to introduce chemical handles useful for late-stage conjugation without affecting the spectroscopic features.

3. Conclusion

Two novel 6-(phenyl)phenanthridine-based complexes, **1** and **2**, were successfully synthesized and fully characterized using single-crystal X-ray diffraction. While both complexes incorporate LˆX ligands featuring pyridyl-triazole and pyridyl-pyrazole groups with comparable molecular geometries, intriguing subtle differences emerged between their crystal structures. Interestingly, **1** showed a non-negligible distortion of the phenanthridine core (atom with maximum deviation from planarity: 0.39 Å; phenyl-phenanthridine inclination: 32.0°). Furthermore, the -OH group of the triazole ring was revealed to be a crucial factor in determining the intermolecular interactions, due to the formation of an H-bond with the neighboring triazole nitrogen atom. Overall, our studies revealed that the molecular geometry is mainly dictated by the 6-(phenyl)phenanthridine CˆN ligand; the slight differences found in the two crystals can be attributed to the different H-bonding abilities of **1**/**2** and to the increase of the number on N atoms in the azole moiety. In line with the crystallographic studies, spectroscopic characterization of the two complexes showed only minor differences in the spectroscopic features of **1** and **2**, thus confirming that the absorption/emission properties also mainly depend on the phenanthridine CˆN ligands.

Accession codes

CCDC accession codes 2393258 and 2407685 contain the supplementary crystallographic data for this paper. This data can be obtained free of charge *via* www.ccdc.cam.ac.uk/data_request/cif, or by emailing data_request@ccdc.cam.ac.uk, or by contacting The Cambridge Crystallographic Data Centre, 12 Union Road, Cambridge CB2 1EZ, UK; fax: +441223 336033.

Declaration of competing interest

The authors declare that they have no known competing financial interests or personal relationships that could have appeared to influence the work reported in this paper.

Acknowledgements

We sincerely thank Prof. Diego Gatta and Dr. Nicola Rotiroti for granting access to their facilities. We also gratefully acknowledge the Mass Spectrometry facility of the Unitech COSPECT at the University of Milan (Italy) to perform the mass spectrometry analyses.

Appendix A. Supplementary data

Supplementary data to this article can be found online at https://doi.org/10.1016/j.ica.2025.122684.

Data availability

Data will be made available on request.

References

[1] E. Longhi, L. De Cola, Iridium(III) complexes for OLED application, in: Iridium(III) in Optoelectronic and Photonics Applications, John Wiley & Sons, Ltd, 2017, pp. 205–274, https://doi.org/10.1002/9781119007166.CH6.
[2] J. Jayabharathi, V. Thanikachalam, S. Thilagavathy, Phosphorescent organic light-emitting devices: iridium based emitter materials – an overview, Coord. Chem. Rev. 483 (2023) 215100, https://doi.org/10.1016/J.CCR.2023.215100.
[3] Y. Zhang, J. Qiao, Near-infrared emitting iridium complexes: molecular design, photophysical properties, and related applications, IScience 24 (2021) 102858, https://doi.org/10.1016/J.ISCI.2021.102858.
[4] H. Gao, M. Qian, X. Yang, S. Ma, H. Li, Recent advances of the cyclometalated iridium(III) complexes for electrochemiluminescence sensing, Dyes Pigments 232 (2025) 112493, https://doi.org/10.1016/J.DYEPIG.2024.112493.
[5] L. Chen, K. Quayle, Z.M. Smith, T.U. Connell, E.H. Doeven, D.J. Hayne, J. L. Adcock, D.J.D. Wilson, J. Agugiaro, M.L. Pattuwage, N.S. Adamson, P.S. Francis, Chemiluminescence and electrochemiluminescence of water-soluble iridium(III) complexes containing a tetraethylene-glycol functionalised triazolylpyridine ligand, Anal. Chim. Acta 1304 (2024) 342470, https://doi.org/10.1016/J.ACA.2024.342470.
[6] A. Fracassa, C.I. Santo, E. Kerr, S. Knežević, D.J. Hayne, P.S. Francis, F. Kanoufi, N. Sojic, F. Paolucci, G. Valenti, Redox-mediated electrochemiluminescence enhancement for bead-based immunoassay, Chem. Sci. 15 (2024) 1150–1158, https://doi.org/10.1039/D3SC06357G.
[7] S. Yoon, T.S. Teets, Enhanced deep red to near-infrared (DR-NIR) phosphorescence in cyclometalated iridium(III) complexes, Inorg. Chem. Front. 9 (2022) 6544–6553, https://doi.org/10.1039/D2QI02058K.
[8] K.M. Kuznetsov, I.S. Kritchenkov, J.R. Shakirova, V.V. Gurzhiy, V.V. Pavlovskiy, V. V. Porsev, V.V. Sokolov, S.P. Tunik, Red-to-NIR iridium(III) emitters: synthesis, Photophysical and computational study, the effects of Cyclometallating and β-Diketonate ligands, Eur J, Inorg. Chem. 2021 (2021) 2163–2170, https://doi.org/10.1002/EJIC.202100189.
[9] M. Penconi, A.B. Kajjam, M.C. Jung, M. Cazzaniga, C. Baldoli, D. Ceresoli, M. E. Thompson, A. Bossi, Advancing near-infrared phosphorescence with Heteroleptic iridium complexes bearing a single emitting ligand: properties and organic light-emitting diode applications, Chem. Mater. 34 (2022) 574–583, https://doi.org/10.1021/ACS.CHEMMATER.1C03030.
[10] S. Lamansky, P. Djurovich, D. Murphy, F. Abdel-Razzaq, R. Kwong, I. Tsyba, M. Bortz, B. Mui, R. Bau, M.E. Thompson, Synthesis and characterization of phosphorescent cyclometalated iridium complexes, Inorg. Chem. 40 (2001) 1704–1711, https://doi.org/10.1021/IC0008969.
[11] S. Yoon, T.G. Gray, T.S. Teets, Enhanced deep-red phosphorescence in Cyclometalated iridium complexes with Quinoline-based ancillary ligands, Inorg. Chem. 62 (2023) 7898–7905, https://doi.org/10.1021/ACS.INORGCHEM.3C00670.
[12] P. Lai, S. Yoon, Y. Wu, T.S. Teets, Effects of ancillary ligands on deep red to near-infrared Cyclometalated iridium complexes, ACS Organic and Inorganic Au 2 (2022) 236–244, https://doi.org/10.1021/ACSORGINORGAU.1C00044.
[13] B. Jiang, Y. Gu, J. Qin, X. Ning, S. Gong, G. Xie, C. Yang, Deep-red iridium(III) complexes cyclometalated by phenanthridine derivatives for highly efficient solution-processed organic light-emitting diodes, J Mater Chem C Mater 4 (2016) 3492–3498, https://doi.org/10.1039/C6TC00148C.
[14] E. Longhi, J.M. Fernandez-Hernandez, A. Iordache, R. Fröhlich, H.P. Josel, L. De Cola, Ir(III) Cyclometalated complexes containing Phenylphenanthridine ligands with different substitutions: effects on the Electrochemiluminescence properties, Inorg. Chem. 59 (2020) 7435–7443, https://doi.org/10.1021/ACS.INORGCHEM.0C00107.
[15] J.M. Fernandez-Hernandez, E. Longhi, R. Cysewski, F. Polo, H.P. Josel, L. De Cola, Photophysics and Electrochemiluminescence of bright Cyclometalated Ir(III) complexes in aqueous solutions, Anal. Chem. 88 (2016) 4174–4178, https://doi.org/10.1021/ACS.ANALCHEM.6B00312.

[16] R. Cysewski, L. De Cola, J.M. Fernandez Hernandez, H.-P. Josel, E. Longhi, G.H. M. Vondenhoff, New Bis-Iridium-Complexes for Manufacturing of ECL-Labels, WO/2014/019710, 2014.
[17] F. Fiorini, E. Longhi, A. Lázaro, D. Di Prisco, G. Tamboia, G. Alonci, L. Menduti, L. De Cola, Label-free 3D cell imaging using hydrogels functionalized with switchable iridium complexes, Chem. Eur. J. (2025) e202404572, https://doi.org/10.1002/CHEM.202404572.
[18] S.W. Youn, J.H. Bihn, Trifluoroacetic acid-mediated facile construction of 6-substituted phenanthridines, Tetrahedron Lett. 50 (2009) 4598–4601, https://doi.org/10.1016/J.TETLET.2009.05.071.
[19] M. Nonoyama, Benzo[h]quinolin-10-yl-N iridium(III) complexes, Bull. Chem. Soc. Jpn. 47 (1974) 767–768, https://doi.org/10.1246/BCSJ.47.767.
[20] J. Roppe, N.D. Smith, D. Huang, L. Tehrani, B. Wang, J. Anderson, J. Brodkin, J. Chung, X. Jiang, C. King, B. Munoz, M.A. Varney, P. Prasit, N.D.P. Cosford, Discovery of novel heteroarylazoles that are metabotropic glutamate subtype 5 receptor antagonists with anxiolytic activity, J. Med. Chem. 47 (2004) 4645–4648, https://doi.org/10.1021/JM049828C.
[21] I.J. Bruno, J.C. Cole, M. Kessler, J. Luo, W.D.S. Momerwell, L.H. Purkis, B.R. Smith, R. Taylor, R.I. Cooper, S.E. Harris, A.G. Orpen, Retrieval of crystallographically-derived molecular geometry information, J. Chem. Inf. Comput. Sci. 44 (2004) 2133–2144, https://doi.org/10.1021/CI049780B.
[22] F.M. Hwang, H.Y. Chen, P.S. Chen, C.S. Liu, Y. Chi, C.F. Shu, F.I. Wu, P.T. Chou, S. M. Peng, G.H. Lee, Iridium(III) complexes with orthometalated quinoxaline ligands: subtle tuning of emission to the saturated red color, Inorg. Chem. 44 (2005) 1344–1353, https://doi.org/10.1021/IC0489443.
[23] D. Schneidenbach, S. Ammermann, M. Debeaux, A. Freund, M. Zöllner, C. Daniliuc, P.G. Jones, W. Kowalsky, H.H. Johannes, Efficient and long-time stable red iridium (III) complexes for organic light-emitting diodes based on quinoxaline ligands, Inorg. Chem. 49 (2010) 397–406, https://doi.org/10.1021/IC9009898.
[24] V.A. Blatov, A.P. Shevchenko, V.N. Serenzhkin, Crystal space analysis by means of Voronoi–Dirichlet polyhedra, Acta Crystallogr. A 51 (1995) 909–916, https://doi.org/10.1107/S0108767395006799.
[25] M. Mori, E. Fumagalli, C. Castellano, A. Tresoldi, A. Sacchetti, F. Meneghetti, Synthesis and characterization of a tetradentate bispidine-based ligand and its zinc (II) complex, Inorg. Chim. Acta 538 (2022) 120968, https://doi.org/10.1016/J.ICA.2022.120968.
[26] V.N. Serezhkin, A.V. Savchenkov, Application of the method of molecular Voronoi-Dirichlet Polyhedra for analysis of noncovalent interactions in aripiprazole polymorphs, Cryst. Growth Des. 20 (2020) 1997–2003, https://doi.org/10.1021/acs.cgd.9b01645.
[27] M. O'Keeffe, IUCr, a proposed rigorous definition of coordination number, Acta Crystallogr. A 35 (1979) 772–775, https://doi.org/10.1107/S0567739479001765.
[28] V. Venkatesan, A. Fujii, N. Mikami, A study on aromatic C–H···X (X = N, O) hydrogen bonds in 1,2,4,5-tetrafluorobenzene clusters using infrared spectroscopy and ab initio calculations, Chem. Phys. Lett. 409 (2005) 57–62, https://doi.org/10.1016/J.CPLETT.2005.04.079.
[29] R. Thakuria, N.K. Nath, B.K. Saha, The nature and applications of π-π interactions: a perspective, Cryst. Growth Des. 19 (2019) 523–528, https://doi.org/10.1021/ACS.CGD.8B01630.
[30] M.A. Spackman, D. Jayatilaka, Hirshfeld surface analysis, CrystEngComm 11 (2009) 19–32, https://doi.org/10.1039/B818330A.
[31] A. Huseynzada, M. Mori, F. Meneghetti, A. Israyilova, G. Tuzun, K. Sayin, L. R. Chiarelli, C. Mutlu, M. Demiralp, U. Hasanova, V. Abbasov, Synthesis, crystal structure, Hirshfeld surface, computational and antibacterial studies of a 9-phenanthrenecarboxaldehyde-based thiodihydropyrimidine derivative, J. Mol. Struct. 1267 (2022) 133571, https://doi.org/10.1016/J.MOLSTRUC.2022.133571.
[32] C. Jelsch, K. Ejsmont, L. Huder, The enrichment ratio of atomic contacts in crystals, an indicator derived from the Hirshfeld surface analysis, IUCrJ 1 (2014) 119–128, https://doi.org/10.1107/S2052252514003327.
[33] I.S. Shin, J. Il Kim, T.H. Kwon, J.I. Hong, J.K. Lee, H. Kim, Efficient electrogenerated chemiluminescence from bis-cyclometalated iridium(III) complexes with substituted 2-phenylquinoline ligands, J. Phys. Chem. C 111 (2007) 2280–2286, https://doi.org/10.1021/JP067644Z.